

In vivo tracking of intravenously injected mesenchymal stem cells in an Alzheimer's animal model

Cell Transplantation
2018, Vol. 27(8) 1203–1209
© The Author(s) 2018
Article reuse guidelines:
sagepub.com/journals-permissions
DOI: 10.1177/0963689718788067
journals.sagepub.com/home/ctj


Bok-Nam Park¹, Tae Sung Lim², Joon-Kee Yoon¹, and Young-Sil An¹

Abstract

Purpose: The purpose of this study was to investigate how intravenously injected bone marrow-derived mesenchymal stem cells (BMSCs) are distributed in the body of an Alzheimer's disease (AD) animal model. **Methods:** Stem cells were collected from bone marrow of mice and labeled with Indium-111 (¹¹¹In). The ¹¹¹In-labeled BMSCs were infused intravenously into 3×Tg-AD mice in the AD group and non-transgenic mice (B6129SF2/J) as controls. Biodistribution was evaluated with a gamma counter and gamma camera 24 and 48 h after injecting the stem cells. **Results:** A gamma count of the brain showed a higher distribution of labeled cells in the AD model than in the control group at 24 (p = .0004) and 48 h (p = .0016) after injection of the BMSCs. Similar results were observed by gamma camera imaging (i.e., brain uptake in the AD model was significantly higher than that in the control group). Among the other organs, uptake by the spleen was the highest in both groups. More BMSCs were found in the lungs of the control group than in those of the AD group. **Conclusions:** These results suggest that more intravenously infused BMSCs reached the brain in the AD model than in the control group, but the numbers of stem cells reaching the brain was very small.

Keywords

Mesenchymal stem cells, Alzheimer's disease, biodistribution, cell tracking

Introduction

Alzheimer's disease (AD) is clinically characterized by memory loss and progressively impaired learning capacity^{1,2}. More patients with AD are expected in an aging society³, so there are concerns about the socioeconomic problems caused by AD. However, current medications for AD have poor efficacy and side effects^{4,5}, so efforts are underway to find new promising therapies.

Therapy using mesenchymal stem cells (MSCs), which can produce a variety of neurotrophic factors and cytokines^{6–8}, has received attention as an important tool to treat various degenerative neurological diseases. In particular, bone marrow-derived MSCs (BMSCs) are relatively free from immune and ethical problems for clinical application^{9–11}. The ultimate goal for stem cell therapy in patients with a neurological disease is recovery of clinical function, which must be initiated by stem cells successfully reaching the host brain. Therefore, studying the tracking and biodistribution of MSCs is important to ensure the safety and efficacy of MSC therapy.

Various labeling methods, including green fluorescent vital dyes, luciferase, iron particles, and radioactivity

labeling, have been attempted for tracking MSCs in previous studies^{12–17}. Of these, radioactivity labeling is a clinically friendly method with the advantage of in vivo imaging. Actually, several previous studies have tracked cells using indium-111 (¹¹¹In) with a relatively long life of 2.80 days in various diseases^{15,18–21}.

Stem cell therapy via the intravenous (IV) route is convenient to apply in clinical practice, so clinicians have become increasingly interested in this method^{22–24}. Despite the fact that some studies have reported that IV-transplanted MSCs can migrate into inflamed and ischemic areas of the brain^{25–27}, the final fate of IV-applied MSCs remains

¹ Department of Nuclear Medicine and Molecular Imaging, Suwon, Korea

² Department of Neurology, Ajou University School of Medicine, Suwon, Korea

Submitted: August 30, 2017. Revised: May 30, 2018. Accepted: June 4, 2018.

Corresponding Author:

Young-Sil An, Department of Nuclear Medicine and Molecular Imaging, School of Medicine, Ajou University, 206, World cup-ro, Yeongtong-gu, Suwon-si, Gyeonggi-do, Suwon 16499, Korea.
Email: aysays77@naver.com



elusive²². We have questioned whether IV-administered MSCs can successfully migrate to the intended target brain tissue in patients with a neurological disease in clinical practice.

Based on these considerations, the present study evaluated the biodistribution of MSCs and determined whether IV-applied, radioactively labeled MSCs could reach the brain in an AD mouse model.

Materials and Methods

Isolation and Culture of Mouse BMSCs

B6129SF2/J mice (Jackson Laboratories, Bar Harbor, ME, USA), weighing 20–25 g, were housed in groups of two or three under environmentally controlled conditions at $23 \pm 2^\circ\text{C}$ and $50 \pm 10\%$ relative humidity and given free access to food and water. All experimental procedures were approved by the Institutional Animal Care and Use Committees of Ajou University School of Medicine, Suwon, Republic of Korea (IACUC No. 2015-0068). The method for BMSC preparation from mice was based on the protocol by Soleimani and Nadri²⁸. Mouse BMSCs were isolated from the femurs of 6–8-week-old female B6129SF2/J mice. Both ends of the tibia and femurs were removed, and the remaining bones were centrifuged at $762 \times g$ for 20 min. The supernatant was discarded, and the cell pellets were resuspended in phosphate-buffered saline (PBS). After centrifugation, the cells were resuspended and incubated in high-glucose Dulbecco modified Eagle's medium containing 15% fetal bovine serum and 1% penicillin/streptomycin (Invitrogen, Carlsbad, CA, USA) at 37°C in a 5% fully humidified CO_2 incubator. Non-adherent cells were removed 18 h later by replacing the medium (passage 0). On day 10 of incubation, the cells were detached with 0.25% trypsin/0.1% EDTA (Sigma, St. Louis, MO, USA) and replated on 100-mm culture dishes (passage 1). When these primary cultures reached 80% confluence, the cells were harvested using 0.25% trypsin and subcultured. Mouse BMSCs were characterized by immunofluorescence and fluorescence-activated cell sorter analysis at passage 4²⁹.

Labeling of Mesenchymal Stem Cells with ¹¹¹In Tropolone

Tropolone (1–2 mg; Sigma) was dissolved in 1 mL of normal saline, and 80 μL of tropolone solution was mixed with 37–111 MBq (1–3 mCi) of ¹¹¹InCl₃ (physical half-life = 2.83 days, γ -energy = 245 and 173 keV; PerkinElmer, Waltham, MA, USA) in 0.05 N HCl. The reaction mixture was incubated for 15 min at room temperature (pH 7.2)³⁰. Before labeling, the BMSCs were washed with PBS, centrifuged at 1000 rpm for 3 min, and resuspended in 1 mL PBS. ¹¹¹In-tropolone was added to the BMSC suspension and incubated at room temperature for 20 min. After the incubation, the BMSCs were centrifuged at 1000 rpm for 3 min, and

the supernatant and cell pellets were collected separately to calculate labeling efficiency.

In Vivo Distribution Using a Gamma Counter and Gamma Camera

¹¹¹In-labeled BMSCs (7.4 MBq, 1.0×10^6 cells/mouse) suspended in 200 μL of normal saline were injected via a tail vein into 3 \times Tg-AD (B6;129-*Psen1*^{tm1Mpm}Tg(APPSwe, tauP301 L)1Lfa/Mmjax, Jackson Laboratories) as the AD group ($n = 28$) and non-transgenic mice (B6129SF2/J) as controls ($n = 25$). The mice were scanned 24 and 48 h after injection with a dual-head gamma camera (Multi-SPECT2, Siemens, Erlangen, Germany) equipped with medium energy collimators for 10 min in the prone position. The matrix size was 256×256 . Circular regions of interest were drawn for the brain and right thigh (background) on both anterior and posterior images, respectively, to compare the biodistribution. The brain uptake ratio was obtained by dividing brain activity by background activity.

Immediately after acquisition, major organs, including the brain, kidneys, lungs, liver, and spleen, were excised and weighed, and radioactivity was measured using a gamma counter (Gamma-HES; Shin Jin Medics Inc., Seoul, Korea). The data are expressed as a percentage of injected dose (%ID/g) after correction for decay.

Immunofluorescence Staining Using Confocal Microscope

To detect intravenously transplanted BMSCs, cells were labeled with PKH26 using a commercial kit (PKH26 red fluorescence cell linker kit, Sigma-Aldrich, St. Louis, MO, USA), according to the manufacturer's instructions³¹. Briefly, cells were centrifuged at $322 \times g$ for 3 min in a conical tube, and the supernatant was discarded. Then 1 mL Diluent C and 4.0×10^{-6} M of PKH26 dye were added to cell pellets, which were incubated at room temperature for 5 min with gentle inversion. Then the mixture was incubated with 2 mL serum for 1 min to stop the staining reaction. Stained cells were centrifuged at $322 \times g$ for 10 min and washed with 10 mL complete medium prior to being further labeled with ¹¹¹In. The radiolabeling and intravenous injection of BMSCs were performed 30 min after PKH26 labeling.

To observe intracerebral BMSCs, brains were harvested from animals and fixed overnight with 4% paraformaldehyde in 0.1 M phosphate buffer. Then the samples were embedded in paraffin blocks and sectioned at 5 μm on a sliding microtome. Sections were deparaffinized by incubating them in an oven for 20 min at 55°C and rinsing three times with PBS (Gibco, Scotts Valley, CA, USA). Next, they were incubated with 4,6-diamidino-2-phenylindole (DAPI) at 1 $\mu\text{L}/\text{mL}$ (Fluka, Morristown, NJ, USA) for 15 min at room temperature to counterstain the nuclei, and then mounted using a cover slide. PKH26 (red) and DAPI (blue) fluorescent signals in tissues were captured and analyzed

Table 1. Biodistribution of ^{111}In -Labeled Stem Cells According to the Gamma Counter.

	Radioactivity (median (interquartile range), %ID/g)					
	24 h after stem cell injection			48 h after stem cell injection		
	AD model	Control	p-value*	AD model	Control	p-value*
Brain	0.31 (0.30–0.33)	0.21 (0.20–0.23)	0.0004	0.38 (0.32–0.40)	0.28 (0.25–0.29)	0.0016
Lungs	18.48 (17.64–19.66)	29.60 (29.35–30.14)	<0.0001	13.06 (9.91–13.56)	16.45 (13.77–18.49)	0.0045
Kidneys	21.87 (21.10–23.54)	18.18 (17.13–19.78)	0.0003	27.19 (24.64–28.88)	15.08 (12.75–16.79)	0.0008
Liver	7.15 (6.87–7.62)	5.10 (4.52–5.79)	0.0031	12.13 (11.24–12.33)	5.38 (4.74–5.88)	0.0005
Spleen	36.29 (35.55–37.20)	35.46 (32.00–38.20)	0.7618	31.78 (31.05–34.14)	55.78 (50.93–56.63)	0.0006

AD: Alzheimer's disease.

*p-value between AD model and control.

using a Nikon A1 confocal laser scanning microscope (Nikon, Tokyo, Japan).

Statistical Analysis

All values were tested for a normal distribution using the Kolmogorov–Smirnov test, and none of the datasets were normal. Thus, non-parametric statistics were used for the data analysis, and all values are presented as median and interquartile range.

To compare the distribution of ^{111}In -labeled BMSCs in each organ between the AD model and controls, radioactivity was analyzed with the Mann–Whitney test. The brain uptake ratio acquired from the gamma camera images was compared between the AD and control models using the Mann–Whitney test. The Wilcoxon test was used to evaluate changes in distribution between 24 and 48 h in both groups. Two-tailed p-values <0.05 were considered significant. MedCalc statistical software ver. 17.6 (MedCalc Software bvba, Ostend, Belgium; <http://www.medcalc.org>; 2017) was used for all statistical analyses.

Results

In Vivo Distribution of ^{111}In -Labeled BMSCs by the Gamma Counter

Radioactivity was measured 24 h after the BMSCs were injected using a gamma counter and revealed that brain uptake was significantly higher in the AD model than in the controls (0.31% vs. 0.21%, $p = 0.0004$). Significant differences in the distributions in the lungs, kidneys, and liver were observed between the AD model and controls 24 h after injection of the BMSCs. Radioactivity in the lungs was significantly higher in the controls than in the AD model, and that in the kidneys and liver was significantly higher in the AD model than in the controls. The distribution in the spleen was not different between the AD and control models 24 h after injection of the BMSCs ($p = 0.7618$).

Brain uptake remained significantly higher in the AD model than in the controls 48 h after injection of the BMSCs (0.38% vs. 0.28%, $p = 0.0016$). Distribution in other organs,

including the lungs, kidneys, liver, and spleen, was significantly different between the two groups 48 h after injection of the BMSCs. The BMSCs were distributed more in the kidneys and liver of the AD model than in the controls. The controls had more BMSCs distributed in the lungs and spleen than the AD model (Table 1).

Changes in the Distribution of BMSCs with Time by the Gamma Counter

The changes in the distribution of BMSCs with time according to the gamma counter are illustrated in Figure 1. Brain uptake in the AD model after 48 h was significantly higher than at 24 h after injection of the BMSCs ($p = 0.0156$). Radioactivity in the lungs and spleen decreased significantly with time, whereas radioactivity in the kidneys and liver increased significantly with time (Figure 1(a)).

Radioactivity in the brain in controls after 48 h was significantly higher than at 24 h after injection of the BMSCs ($p = 0.0039$). BMSCs in the kidneys and lungs decreased significantly with time in the control group, whereas radioactivity in the spleen increased significantly with time. The distribution in the liver did not change significantly with time ($p = 0.6250$, Figure 1(b)).

Brain Uptake by the Gamma Camera

On gamma camera images, ^{111}In -labeled BMSC uptake in the brains of the AD model was significantly higher 24 h after injection of the BMSCs than that in the controls (2.53 vs. 1.54, $p < 0.0001$, Figure 2(a)). Significantly more brain uptake was noted in the AD model than in the controls 48 h after administration of the BMSCs (2.67 vs. 1.53, $p < 0.0001$, Figure 2(a)).

Brain uptake increased significantly with time in the AD model when the 24 and 48 h images were compared ($p = 0.0017$, Figure 2(a)). However, brain uptake did not change significantly with time in the controls ($p = 0.3394$, Figure 2(a)).

Representative gamma camera images are shown in Figure 2(b) and (c).

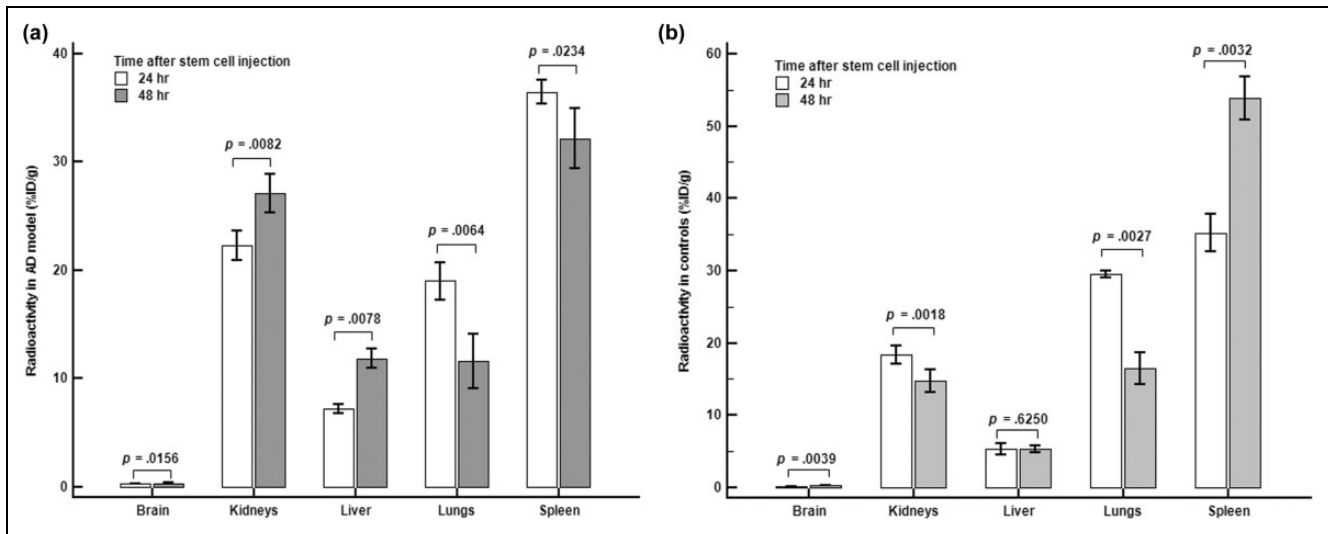


Figure 1. Comparison of radioactivity 24 and 48 h after stem cells were injected according to the gamma counter. (a) Significant increases in radioactivity were seen in the brain, kidneys, and liver of the AD model, whereas that in the lungs and spleen decreased with time. (b) Radioactivity in the brain and spleen increased significantly with time in the control group, whereas that in the kidneys and liver decreased significantly. Liver radioactivity did not change significantly with time.

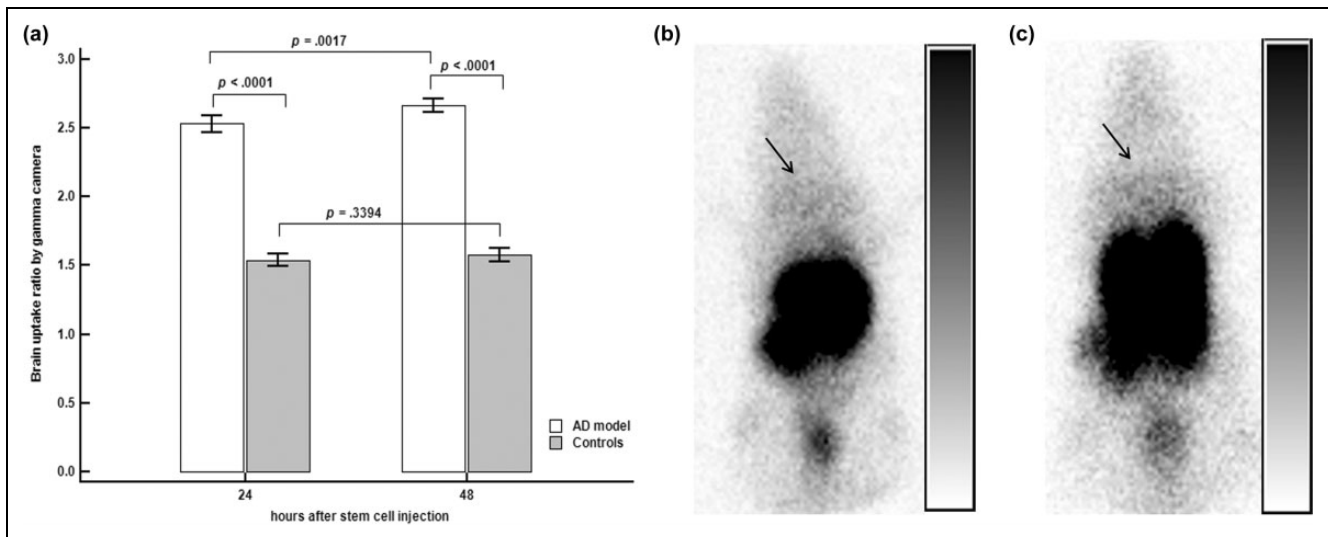


Figure 2. Brain uptake by gamma camera. (a) The brain uptake ratio was significantly higher in the Alzheimer's disease (AD) model than in the controls 24 and 48 h after stem cell injection. Brain uptake in the AD model increased significantly with time, but no significant changes were observed with time in the control group. (b) Representative image in the AD model 48 h after stem cell injection; slightly increased uptake can be observed in the brain region, as indicated by the arrow. (c) An arrow indicates that they also showed a slight increase in brain uptake in a representative control image 48 h after stem cell injection. Although the visual activity of the brain in (b) and (c) seemed to be similar, the uptake ratio showed significant differences between the two groups (2.67 vs. 1.53, $p < 0.0001$).

Confocal Microscopic Analysis of Transplanted BMSCs

To further confirm that MSCs were homing to the brain following injection into the tail vein, we employed immunofluorescence staining. Confocal microscopy confirmed the presence of PKH26- ^{111}In co-labeled BMSCs in the AD brain tissue (Figure 3). This confocal microscopy image revealed that BMSCs labeled with ^{111}In migrated to AD brains within

24 h after injection, and that the migration ability of BMSCs was not affected by ^{111}In .

Discussion

The therapeutic effects of MSCs in models of AD have been revealed by various studies^{32–38}. Several effects have been reported, including inhibition of cell death³², reduction of

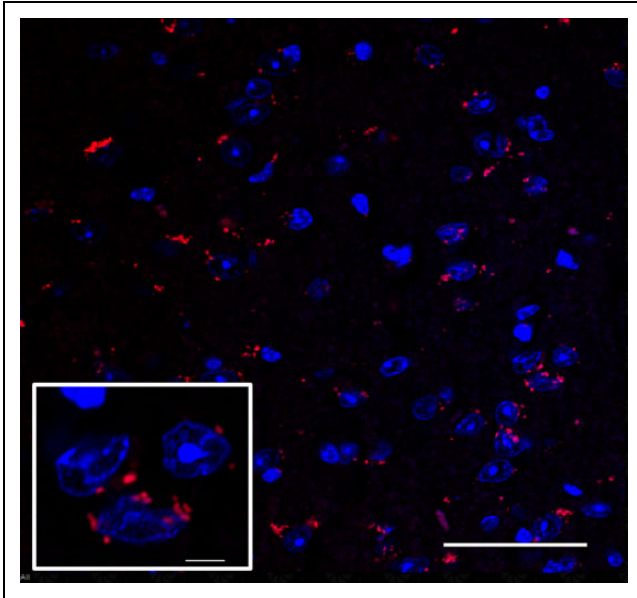


Figure 3. Migration of transplanted PKH26-¹¹¹In co-labeled BMSCs into the brain of AD mice. A confocal image showing that intravenously injected stem cells were successfully found in brain tissue of the AD model. Blue: DAPI; red: PKH26; scale bar = 5 μ m; magnification: $\times 60$ for larger images, $\times 470$ for small images.

amyloid deposits³⁷, and rescue of learning and memory deficits^{33,38}, which may be induced by the neuroprotective paracrine effects of MSC-secreted factors^{39,40}. Although Naaldijk et al.³⁶ reported the therapeutic effects of IV-injected MSCs in the AD model, there is still a concern about the delivery of MSCs to the brain via IV administration. In this context, we investigated whether IV-injected MSCs would reach the brain using a radioactive isotope labeling method.

This study confirmed that a small number of the BMSCs injected IV into AD mice reached the brain. Radioactivity of BMSCs was significantly higher in the AD model than in the control group according to the gamma counter and gamma camera imaging. It is very difficult to know why the BMSCs were more distributed in the brains of the AD model than in the controls, because few previous studies have been conducted for the same purpose. We believe that the distribution of stem cells in the body may differ depending on the disease model.

The choice of animal model for preclinical studies using stem cells is critical. In addition, the first step in studying biodistribution is to use MSCs from the same animal species⁴¹. We used 3 \times Tg-AD mice as the AD model and B6129SF2/J mice as the control in this study. The 3 \times Tg-AD mice have been successfully used in previous stem cell studies^{42–44}. The B6129SF2/J mice have been suggested to be the best control mice to use for studying 3 \times Tg-AD mice⁴⁵. We used MSCs from B6129SF2/J bone marrow, which would ideally be sourced from the same species as the 3 \times Tg-AD model.

Previous studies have reported that IV-injected stem cells are mainly distributed in the lungs, liver, and spleen^{22,46,47}, and these results are not significantly different from the results of our study. Notably, the distribution of BMSCs in the lungs was relatively low in the AD model compared with the control group. The most problematic aspect of IV stem cell therapy is the initial pulmonary entrapment, and the accumulation of stem cells in lungs is a key determining factor for their biodistribution^{15,22,41,48}. Thus, the low lung uptake that we observed in the AD model may be a meaningful result. We suggest, after careful consideration, that this is related to the relatively higher brain intake in the AD model than in the control group. These results suggest that the distribution of BMSCs in the brain and other organs may vary depending on the type of mouse model.

¹¹¹In is a radioactive isotope with a relatively long half-life of 2.8049 days. Therefore, in our study, the distribution of BMSCs was traced for a relatively long period after injection. We were able to follow the changes in BMSC distribution over time, and, as a result, radioactivity in the lung decreased with time in both models. Radioactivity was higher in the kidneys of the AD model over time, whereas radioactivity in the control group kidneys was lower. Liver radioactivity increased over time in the AD model, and uptake by the spleen increased in the control group. These changes in distribution over time may be explained by secondary recirculation of stem cells, and this recirculation could differ depending on the disease model or species, which is consistent with our results⁴¹.

A higher distribution of BMSCs was observed in the brain of the AD model than the control group according to the gamma camera images. The imaging results also showed that brain uptake did not change significantly over time in the control group, whereas brain uptake increased in the AD group. Stem cells have never been tracked with gamma camera images in an AD model as shown in this study. We obtained confocal microscopy images to confirm that the radioactivity of the brain visible in the gamma camera represented real stem cells, and we identified BMSCs in brain parenchymal tissue. In Naaldijk et al.³⁶, confocal images showed that IV-injected stem cells had reached the brain of APP/PS1 mice, an AD animal model. Our results are consistent with those findings.

A limitation of this study is that the gamma camera images were acquired using human equipment. The research institute did not have a gamma camera for small animals, so we obtained the best images possible using a camera for humans, but quality was inferior. In addition, because of limitations of the camera resolution, it was difficult to evaluate the distribution of images in other organs except the brain. A further tracking study using a more advanced animal-specific gamma camera such as single photon emission computed tomography might be needed to validate our results.

In conclusion, this study suggests that a small number of stem cells injected IV in an AD model can reach the brain.

Ethical Approval

All experimental procedures were approved by the Institutional Animal Care and Use Committees of Ajou University School of Medicine, Suwon, Republic of Korea (IACUC No. 2015-0068).

Statement of Human and Animal Rights

The method for BMSC preparation from mice was based on the protocol by Soleimani and Nadri.

Statement of Informed Consent

Statement of Informed Consent is not applicable for this article.

Declaration of Conflicting Interests

The authors declared no potential conflicts of interest with respect to the research, authorship, and/or publication of this article.

Funding

The authors disclosed receipt of the following financial support for the research and/or authorship of this article: This work was supported by a National Research Foundation of Korea (NRF) grant, funded by the Korean government (MEST) (NRF-2015R1C1A2A01052005).

References

- Terry RD, Masliah E, Salmon DP, Butters N, DeTeresa R, Hill R, Hansen LA, Katzman R. Physical basis of cognitive alterations in Alzheimer's disease: synapse loss is the major correlate of cognitive impairment. *Ann Neurol*. 1991;30(4):572–80.
- Cummings JL. Cognitive and behavioral heterogeneity in Alzheimer's disease: seeking the neurobiological basis. *Neurobiol Aging*. 2000;21(6):845–61.
- Oliveira AA Jr, Hodges HM. Alzheimer's disease and neural transplantation as prospective cell therapy. *Curr Alzheimer Res*. 2005;2(1):79–95.
- Akhondzadeh S, Noroozian M. Alzheimer's disease: pathophysiology and pharmacotherapy. *IDrugs*. 2002;5(11):1062–9.
- Bachurin SO. Medicinal chemistry approaches for the treatment and prevention of Alzheimer's disease. *Med Res Rev*. 2003;23(1):48–88.
- Wilkins A, Kemp K, Ginty M, Hares K, Mallam E, Scolding N. Human bone marrow-derived mesenchymal stem cells secrete brain-derived neurotrophic factor which promotes neuronal survival in vitro. *Stem Cell Res*. 2009;3(1):63–70.
- Nomura T, Honmou O, Harada K, Houkin K, Hamada H, Kocsis JD. IV infusion of brain-derived neurotrophic factor gene-modified human mesenchymal stem cells protects against injury in a cerebral ischemia model in adult rat. *Neurosci*. 2005;136(1):161–9.
- Crigler L, Robey RC, Asawachaicharn A, Gaupp D, Phinney DG. Human mesenchymal stem cell subpopulations express a variety of neuro-regulatory molecules and promote neuronal cell survival and neurogenesis. *Exp Neurol*. 2006;198(1):54–64.
- Ballas CB, Zielske SP, Gerson SL. Adult bone marrow stem cells for cell and gene therapies: implications for greater use. *J Cell Biochem*. 2002;85(S38):20–8.
- Pittenger MF, Mackay AM, Beck SC, Jaiswal RK, Douglas R, Mosca JD, Moorman MA, Simonetti DW, Craig S, Marshak DR. Multilineage potential of adult human mesenchymal stem cells. *Science*. 1999;284(5411):143–7.
- Frankel MS. In search of stem cell policy. *Science*. 2000;287(5457):1397.
- Devine SM, Bartholomew AM, Mahmud N, Nelson M, Patil S, Hardy W, Sturgeon C, Hewett T, Chung T, Stock W, Sher D, Weissman S, Ferrer K, Mosca J, Deans R, Moseley A, Hoffman R. Mesenchymal stem cells are capable of homing to the bone marrow of non-human primates following systemic infusion. *Exp Hematol*. 2001;29(2):244–55.
- Devine SM, Cobbs C, Jennings M, Bartholomew A, Hoffman R. Mesenchymal stem cells distribute to a wide range of tissues following systemic infusion into nonhuman primates. *Blood*. 2003;101(8):2999–3001.
- Gao J, Dennis JE, Muzic RF, Lundberg M, Caplan AI. The dynamic in vivo distribution of bone marrow-derived mesenchymal stem cells after infusion. *Cells Tissues Organs*. 2001;169(1):12–20.
- Barbash IM, Chouraqui P, Baron J, Feinberg MS, Etzion S, Tessone A, Miller L, Guetta E, Zipori D, Keddes LH, Kloner RA, Leor J. Systemic delivery of bone marrow-derived mesenchymal stem cells to the infarcted myocardium. *Circulation*. 2003;108(7):863–8.
- Kraitchman DL, Tatsumi M, Gilson WD, Ishimori T, Kedziorrek D, Walczak P, Segars WP, Chen HH, Fritzges D, Izbudak I, Young RG, Marcelino M, Pittenger MF, Solaiyappan M, Boston RC, Tsui BM, Wahl RL, Bulte JW. Dynamic imaging of allogeneic mesenchymal stem cells trafficking to myocardial infarction. *Circulation* 2005;112(10):1451–61.
- Karp JM, Teo GSL. Mesenchymal stem cell homing: the devil is in the details. *Cell Stem Cell*. 2009;4(3):206–16.
- Brenner W, Aicher A, Eckey T, Massoudi S, Zuhayra M, Koehl U, Heeschen C, Kampen WU, Zeiher AM, Dimmeler S, Henze E. ¹¹¹In-labeled CD34+ hematopoietic progenitor cells in a rat myocardial infarction model. *J Nucl Med*. 2004;45(3):512–18.
- Chin BB, Nakamoto Y, Bulte JW, Pittenger MF, Wahl R, Kraitchman DL. ¹¹¹In oxine labelled mesenchymal stem cell SPECT after intravenous administration in myocardial infarction. *Nucl Med Commun*. 2003;24(11):1149–54.
- Jin Y, Kong H, Stodilka RZ, Wells RG, Zabel P, Merrifield PA, Sykes J, Prato FS. Determining the minimum number of detectable cardiac-transplanted ¹¹¹In-tropolone-labelled bone-marrow-derived mesenchymal stem cells by SPECT. *Phys Med Biol*. 2005;50(19):4445–55.
- Yoon JK, Park BN, Shim WY, Shin JY, Lee G, Ahn YH. In vivo tracking of ¹¹¹In-labeled bone marrow mesenchymal stem cells in acute brain trauma model. *Nucl Med Biol*. 2010;37(3):381–8.
- Leibacher J, Henschler R. Biodistribution, migration and homing of systemically applied mesenchymal stem/stromal cells. *Stem Cell Res Ther*. 2016;7(1):7.
- Horwitz EM, Gordon PL, Koo WKK, Marx JC, Neel MD, McNall RY, Muul L, Hofmann T. Isolated allogeneic bone marrow-derived mesenchymal cells engraft and stimulate growth in children with osteogenesis imperfecta: implications for cell therapy of bone. *Proc Natl Acad Sci*. 2002;99(13):8932–7.

24. Horwitz EM, Prockop DJ, Fitzpatrick LA, Koo WW, Gordon PL, Neel M, Sussman M, Orchard P, Marx JC, Pyeritz RE, Brenner MK. Transplantability and therapeutic effects of bone marrow-derived mesenchymal cells in children with osteogenesis imperfecta. *Nat Med*. 1999;5(3):309–13.
25. Wu J, Sun Z, Sun HS, Wu J, Weisel RD, Keating A, Li ZH, Feng ZP, Li RK. Intravenously administered bone marrow cells migrate to damaged brain tissue and improve neural function in ischemic rats. *Cell Transplant*. 2007;16(10):993–1005.
26. Yilmaz G, Vital S, Yilmaz CE, Stokes KY, Alexander JS, Granger DN. Selectin-mediated recruitment of bone marrow stromal cells in the posts ischemic cerebral microvasculature. *Stroke*. 2011;42(3):806–11.
27. Wei L, Fraser JL, Lu ZY, Hu X, Yu SP. Transplantation of hypoxia preconditioned bone marrow mesenchymal stem cells enhances angiogenesis and neurogenesis after cerebral ischemia in rats. *Neurobiol Dis*. 2012;46(3):635–45.
28. Soleimani M, Nadri S. A protocol for isolation and culture of mesenchymal stem cells from mouse bone marrow. *Nat Protoc*. 2009;4(1):102–6.
29. Park HJ, Lee PH, Bang OY, Lee G, Ahn YH. Mesenchymal stem cells therapy exerts neuroprotection in a progressive animal model of Parkinson's disease. *J Neurochem*. 2008;107(1):141–51.
30. Gunter KP, Lukens JN, Clanton JA, Morris PJ, Janco RL, English D. Neutrophil labeling with indium-111: tropolone vs. oxine. *Radiology*. 1983;149(2):563–6.
31. Wallace PK, Tario JD, Fisher JL, Wallace SS, Ernstoff MS, Muirhead KA. Tracking antigen-driven responses by flow cytometry: monitoring proliferation by dye dilution. *Cytometry A*. 2008;73(11):1019–34.
32. Zilka N, Zilkova M, Kazmerova Z, Sarissky M, Cigankova V, Novak M. Mesenchymal stem cells rescue the Alzheimer's disease cell model from cell death induced by misfolded truncated tau. *Neuroscience*. 2011;193:330–7.
33. Lee HJ, Lee JK, Lee H, Carter JE, Chang JW, Oh W, Yang YS, Suh JG, Lee BH, Jin HK, Bae JS. Human umbilical cord blood-derived mesenchymal stem cells improve neuropathology and cognitive impairment in an Alzheimer's disease mouse model through modulation of neuroinflammation. *Neurobiol Aging*. 2012;33(3):588–602.
34. Oh SH, Kim HN, Park HJ, Shin JY, Lee PH. Mesenchymal stem cells increase hippocampal neurogenesis and neuronal differentiation by enhancing the Wnt signaling pathway in an Alzheimer's disease model. *Cell Transplant*. 2015;24(6):1097–109.
35. Duncan T, Valenzuela M. Alzheimer's disease, dementia, and stem cell therapy. *Stem Cell Res Ther*. 2017;8(1):111.
36. Naaldijk Y, Jäger C, Fabian C, Leovsky C, Blüher A, Rudolph L, Hinze A, Stolzing A. Effect of systemic transplantation of bone marrow-derived mesenchymal stem cells on neuropathology markers in APP/PS1 Alzheimer mice. *Neuropathol Appl Neurobiol*. 2017;43(4):299–314.
37. Yun HM, Kim HS, Park KR, Shin JM, Kang AR, Il Lee K, Song S, Kim YB, Han SB, Chung HM, Hong JT. Placenta-derived mesenchymal stem cells improve memory dysfunction in an Aβ1–42-infused mouse model of Alzheimer's disease. *Cell Death Dis*. 2013;4(12):e958.
38. Yang H, Xie ZH, Wei LF, Yang HN, Yang SN, Zhu ZY, Wang P, Zhao CP, Bi JZ. Human umbilical cord mesenchymal stem cell-derived neuron-like cells rescue memory deficits and reduce amyloid-beta deposition in an AβPP/PS1 transgenic mouse model. *Stem Cell Res Ther*. 2013;4(4):76.
39. Munoz JR, Stoutenger BR, Robinson AP, Spees JL, Prockop DJ. Human stem/progenitor cells from bone marrow promote neurogenesis of endogenous neural stem cells in the hippocampus of mice. *Proc Natl Acad Sci U S A*. 2005;102(50):18171–6.
40. Teixeira FG, Carvalho MM, Neves-Carvalho A, Panchalingam KM, Behie LA, Pinto L, Sousa N, Salgado AJ. Secretome of mesenchymal progenitors from the umbilical cord acts as modulator of neural/glial proliferation and differentiation. *Stem Cell Rev*. 2015;11(2):288–97.
41. Sensebé L, Fleury-Cappellesso S. Biodistribution of mesenchymal stem/stromal cells in a preclinical setting. *Stem Cells Int*. 2013;2013:1–5.
42. Blurton-Jones M, Kitazawa M, Martinez-Coria H, Castello NA, Müller F-J, Loring JF, Yamasaki TR, Poon WW, Green KN, LaFerla FM. Neural stem cells improve cognition via BDNF in a transgenic model of Alzheimer disease. *Proc Natl Acad Sci*. 2009;106(32):13594–9.
43. Jensen MM, Arvaniti M, Mikkelsen JD, Michalski D, Pinborg LH, Härtig W, Thomsen MS. Prostate stem cell antigen interacts with nicotinic acetylcholine receptors and is affected in Alzheimer's disease. *Neurobiol Aging*. 2015;36(4):1629–38.
44. Yamamoto S, Ooshima Y, Nakata M, Yano T, Matsuoka K, Watanabe S, Maeda R, Takahashi H, Takeyama M, Matsumoto Y, Hashimoto T. Generation of gene-targeted mice using embryonic stem cells derived from a transgenic mouse model of Alzheimer's disease. *Transgenic Res*. 2013;22(3):537–47.
45. Gstir R, Schaffner S, Scheideler M, Misslinger M, Griehl M, Daschil N, Humpel C, Obermair GJ, Schmuckermair C, Striessnig J, Flucher BE, Hüttenhofer A. Generation of a neuro-specific microarray reveals novel differentially expressed noncoding RNAs in mouse models for neurodegenerative diseases. *RNA*. 2014;20(12):1929–43.
46. Koç ON, Gerson SL, Cooper BW, Dyhouse SM, Haynesworth SE, Caplan AI, Lazarus HM. Rapid hematopoietic recovery after coinfusion of autologous-blood stem cells and culture-expanded marrow mesenchymal stem cells in advanced breast cancer patients receiving high-dose chemotherapy. *J Clin Oncol*. 2000;18(2):307–16.
47. Gholamrezanezhad A, Mirpour S, Bagheri M, Mohamadnejad M, Alimoghaddam K, Abdolhazadeh L, Saghari M, Malekzadeh R. In vivo tracking of ¹¹¹In-oxine labeled mesenchymal stem cells following infusion in patients with advanced cirrhosis. *Nucl Med Biol*. 2011;38(7):961–7.
48. Kang WJ, Kang HJ, Kim HS, Chung JK, Lee MC, Lee DS. Tissue distribution of 18F-FDG-labeled peripheral hematopoietic stem cells after intracoronary administration in patients with myocardial infarction. *J Nucl Med*. 2006;47(8):1295–301.